Journal of the Serbian Chemical Society
JSCS@tmf.bg.ac.rs • www.shd.org.rs/JSCS
J. Serb. Chem. Soc. *88* (12) 1335–1354 (2023)
JSCS–5699
Original scientific paper
Published 19 December 2023

Synthesis, spectroscopic characterization and DFT analysis of dichlorido(η^6-*p*-cymene)ruthenium(II) complexes with isonicotinate-polyethylene glycol ester ligands

THOMAS EICHHORN[1•], DUŠAN DIMIĆ[2•#], ZORAN MARKOVIĆ[3] and GORAN N. KALUĐEROVIĆ[1*]

[1]*Department of Engineering and Natural Sciences, University of Applied Sciences Merseburg, Eberhard-Leibnitz-Straße 2, 06217 Merseburg, Germany,* [2]*University of Belgrade, Faculty of Physical Chemistry, Studentski trg 12–16, 11000 Belgrade, Serbia and* [3]*Institute of Information Technologies, University of Kragujevac, Jovana Cvijića bb, 34000 Kragujevac, Serbia*

(Received 12 April, revised 26 June, accepted 18 September 2023)

Abstract: Ruthenium complexes have gained significant attention due to the ruthenium similarity to iron, lower toxicity, and higher anticancer effectiveness than other compounds. In this contribution, five new isonicotinate-polyethylene glycol ester ligands were synthesised and characterised by NMR and IR spectroscopies. The corresponding Ru(II) complexes were also obtained, and their structure was investigated by traditional methods. The optimisation of structures was performed at B3LYP/6-31+G(d,p) level of theory for H, C, N and O atoms and B3LYP/LanL2DZ for Ru. The intramolecular stabilisation interactions were assessed through the natural bond orbital approach. The NMR chemical shifts were predicted by the gauge independent atomic orbital method and compared to the experimental values. High correlation coefficients and low mean absolute errors between these data sets proved that the predicted structures described well the experimental ones. The theoretical and experimental IR spectra were also compared, and differences in the most notable bands were described. One of the ligands (**L5**) and complexes (**5**) showed fluorescent properties due to methylisatoic moiety. The electronic spectra of this compound were modelled by the time dependent-density functional theory method. The difference of 11 nm between the experimental and the theoretical wavelength was explained by the interactions between the solvent and the solute. Further biological and theoretical studies are advised for this series of compounds.

Keywords: ruthenium(II) complexes; DFT; NBO; isonicotinate; IR; NMR.

* Corresponding author. E-mail: goran.kaluderovic@hs-merseburg.de
• Equaly contributed.
Serbian Chemical Society member.
https://doi.org/10.2298/JSC230412070E

INTRODUCTION

Cancer is a leading cause of death worldwide, representing a multifactorial and complex disease. The discovery of cisplatin in the 60s of the twentieth century marked the beginning of using complex compounds in treating different cancers.[1] Although proven effective, this compound has some severe side effects, including myelosuppression, emesis, nephrotoxicity and alopecia, besides possible inherent resistance observed in some cancer types.[1,2] Therefore, the attention has been focused on similar compounds with higher effectiveness and lower toxicity. Complexes based on platinum-type metals, such as palladium, ruthenium, iridium, rhodium and osmium, represent possible substitutes for cisplatin.[3–5] Due to its similarity in chemical behaviour to iron, ruthenium is characterised by higher human organism tolerance and higher selectivity. *In vitro* studies[6] focus mostly on Ru(II)-arene and Ru(II)-polypyridine complexes.

The development of so-called "half sandwich" Ru(II)-arene compounds (or "piano-stool" complexes) is underway as these compounds offer diversity in the possible substituents that influence the biological activity.[4,7] The general formula of these compounds is [(η^6-arene)Ru(*YZ*)(*X*)], in which *YZ* can be either a bidentate ligand or two monodentate ligands.[7] Compounds having neutral monodentate ligands commonly contain, beside η^6-arene, two chlorido ligands. The solubility of Ru(II) complexes in water represented a severe drawback for their application in medicine. The ionic complexes have much greater potential, and the research nowadays focuses on the compounds with the increased halide ligands groups.[8,9] Some of the examples of Ru(III) compounds that entered clinical trials are imidazolium *trans*-[tetrachlorido(dimethyl sulfoxide)(1-*H*-imidazole)ruthenate(III)] (NAMI-A), indazolium *trans*-[tetrachloridobis(1-*H*-indazole)ruthenate(III)] (KP1019) and their sodium analogues.[1] Depending on the choice of ligands, Ru(II) compounds also possess some antiradical activity towards the reactive species, such as hydroxyl radical.[10]

The coordination properties of nicotinic and isonicotinic acid to lanthanide ions were described 1970s.[11] The study by Schobert and Biersack investigated *cis*-dichloridoplatinum(II) complexes with aminomethylnicotinate and isonicotinate ligands, in which these compounds acted as bidentate ligands.[12] Rhenium(I)--polypyridine complexes coordinated to ethyl-isonicotinate exhibited luminescence that depended on polypyridine moiety and that could be used as photosensitizers for the singlet oxygen production in cells.[13] Mixed metal complexes of copper(II) and vanadium(V) incorporating isonicotinate ligands were obtained by Wang and coworkers.[14] Four new uranium(VI) isonicotinate framework solids had a range of dimensionalities from zero-dimensional to two-dimensional compounds and were described by Kim and coworkers.[15]

This research aims to describe the synthesis and structural characterization of five new isonicotinate-polyethylene glycol ester ligands and their correspond-

ing Ru(II) complexes. NMR, IR, MS, UV–Vis, fluorescence spectroscopies and elemental analysis are used in this contribution to determine the structures of compounds. The structures of the obtained compounds were also validated by predicting IR, NMR and UV–Vis spectra calculated using the density functional theory (DFT) results and comparing them with the experimental ones. Interactions governing the stability of ligands and complexes are also examined in detail by the natural bond orbital (NBO) theory.

EXPERIMENTAL AND THEORETICAL METHODS

Materials and methods

Preparative technique. Ligand precursors were prepared in dry toluene and acetonitrile. All reactions of ruthenium(II) complexes were carried out under argon by using the standard Schlenk line technique. Diethyl ether and toluene were distilled from sodium benzophenone. Dichloromethane was distilled from calcium hydride. 2-Propanol was dried with molecular sieve 3 Å and degassed with argon before use. Ethylene glycol was freshly distilled and stored with a molecular sieve 4 Å. All other poly(ethylene oxide) compounds and poly(ethylene oxide) monomethyl ethers were dried with sodium sulphate. Ligand precursor (**L1**·HCl) and appropriate ruthenium(II) complex (**1**) were previously reported[16] and used here for comparison and theoretical calculations.

Purchased materials. Isonicotinic acid, thionyl chloride, diethylene glycol and α-terpinene were purchased from Acros Organics. Triethylene glycol, tetraethylene glycol and diethylene glycol monomethyl ether were ordered from Merck. Glycol monomethyl ether and triethylene glycol monomethyl ether were purchased from Fluka. Ruthenium(III) chloride hydrate was also commercially available from Alfa Aesar.

Instrumental methods

All samples were measured in 5 mm NMR tubes at 300 K; other conditions are noted. ^{1}H- and ^{13}C-NMR spectra were recorded on Varian Unity 500 or Varian Gemini 400 spectrometers. The chemical shift of ^{1}H-NMR spectra is relative to signals of undeuterated solvents, C*H*Cl$_3$ (δ = 7.26 ppm) and *H*DO (δ = 4.79 ppm). ^{13}C-NMR spectra are calibrated to solvent *C*DCl$_3$ (δ = 77.16 ppm) and all signals noted in the experimental part are singlets. IR spectra were measured from 4000–250 cm^{-1} with a Bruker Tensor 27 FT-IR-spectrometer with diamond ATR. High-resolution ESI mass spectra were obtained from a Bruker Apex III Fourier transform ion cyclotron resonance (FTR-ICR) mass spectrometer (Bruker Daltonics) equipped with an infinity cell, a 7.0 T superconducting magnet (Bruker), an rf-only hexapole ion guide and an external Apollo electrospray ion source (Agilent, off-axis spray). The sample solutions were introduced continuously via a syringe pump with a flow rate of 120 μL h^{-1}. The ligand precursors are noted without hydrochloride as [M+H]$^+$. UV–Vis spectra were recorded on an HP 8453 (Hewlett–Packard GmbH, Waldbronn Analytical Division, Germany), and the fluorescence spectra were recorded on the Fluoromax 2 (Horiba Jobin Yvon GmbH, Unterhaching, Germany). All measurements were performed at room temperature and in cuvettes from Hellma GmbH & Co. KG (Müllheim, Germany, d = 1 cm).

Theoretical methods

All structures were optimized using the Gaussian 09 Program Package[17] without any geometrical constraints. The global hybrid generalised gradient approximation (GAA) functional B3LYP[18] and 6-311++G(d,p)[19] basis set was employed to optimize the ligand structure.

Ligands were optimized in protonated form to follow the experimentally obtained hydrochloride salts. For Ru(II) complexes, B3LYP functional in conjunction with the basis sets 6-31++G(d,p) for H, C, N and Cl, and LanL2DZ[20,21] were employed. The absence of imaginary frequencies showed that the minima of the potential energy surface were obtained. The vibrational frequencies were analysed and visualized in the GausView program.[22] The correction factors for the selected level of theory were obtained on the National Institute of Standards and Technology website (https://cccbdb.nist.gov/vsfx.asp). The influence of solvents on the simulated NMR (D_2O, $CDCl_3$) and UV–Vis (H_2O) spectra was simulated using the Conductor-like polarizable continuum model (CPCM).[23] The intramolecular interactions governing structure stability were analysed by the natural bond orbital[24] (NBO) approach, as implemented in the Gaussian Program package. The ^{1}H- and ^{13}C-NMR chemical shifts were calculated by the gauge independent atomic orbital (GIAO)[25,26] Approach. The TMS as an internal standard for NMR measurements was also optimised at the mentioned level of theory, and NMR spectra were predicted. The electronic transitions were calculated by the time dependent-density functional theory (TD-DFT).[27]

*General procedure for the synthesis of isonicotinate esters (**L2**·HCl–**L5**·HCl)*

The isonicotinic acid (Table I), and dimethylformamide (0.03 g, 0.4 mmol) were cooled to 15 °C, and the excess thionyl chloride (5 mL, 70 mmol) was added dropwise. The reaction mixture was stirred at 40 °C for one hour. The formed light yellow acyl chloride hydrochloride was obtained by evaporating the solvent and the rest of the thionyl chloride and dried *in vacuo*. The obtained acyl chloride hydrochloride was used *in situ* to prepare poly(ethylene glycol) esters (Fig. 1). The acyl chloride hydrochloride was suspended in toluene (40 mL). The appropriate poly(ethylene oxide) monomethyl ether was added at 15 °C and stirred overnight at room temperature. The product precipitated during the reaction was filtered off and washed with toluene (recrystallization from ethanol, method A). If viscous oils were obtained, toluene was removed *in vacuo* and impurities were removed by the extraction with acetone/diethyl ether (method B).

Properties, analytical and spectral data of the synthesized compounds are given in Supplementary material to this paper.

TABLE I. Reaction details for the preparation of ruthenium(II) complexes **2**–**5**

Complex	n({$RuCl_2(\eta^6$-*p*-cymene)$\}_2$) mmol	n(**L2**·HCl–**L5**) mmol	Reaction time, h	Yield, %
2	0.10	0.22	1	96
3	0.10	0.24	1	97
4	0.15	0.37	2	72
5	0.055	0.113	2	65

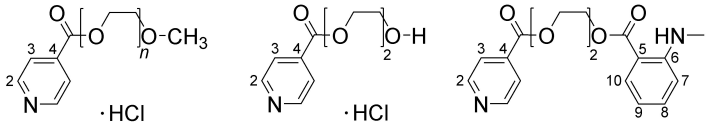

Fig. 1. Poly(ethylene oxide) monomethyl ether (n 1–3) esters of isonicotinic acid (**L1**·HCl–**L3**·HCl), di(ethylene oxide) monoester of isonicotinic acid (**L4**·HCl) and fluorescent ligand (**L5**) with assignment for NMR characterization.

*2-(2-Hydroxyethoxy)ethyl isonicotinate hydrochloride (**L4**·HCl)*. Isonicotinic acid (1.23 g, 10 mmol) and dimethylformamide (0.03 g, 0.4 mmol) were cooled to 15 °C, and the excess thionyl chloride (5 mL, 70 mmol) was added slowly. The suspension was stirred, heated to 40 °C for 1 h and turned light yellow. The formed isonicotinic acyl chloride hydrochloride was obtained by evaporation of the reaction mixture, dried *in vacuo*, and used *in situ* to prepare **L4**·HCl.

The isonicotinic acyl chloride hydrochloride was suspended in toluene (20 mL). Diethylene glycol (5.7 mL, 60 mmol) was added and the mixture was stirred overnight at rt. The crude product precipitated during the reaction, and toluene was removed *in vacuo*. The product was extracted with acetone/diethyl ether and multiple times redissolved in acetone and precipitated with excess diethyl ether. Yield: 0.34 g (14 %).

*2-[2-(2-Methylamino-benzoyloxy)ethoxy]ethyl isonicotinate (**L5**)*. **L4**·HCl (62 mg, 0.25 mmol), methylisatoic acid anhydride (54.3 mg, 0.31 mmol) and potassium carbonate (60 mg, 0.5 mmol) were suspended in acetonitrile (20 mL) and stirred at 60 °C for 3 h. The precipitate was filtered off and washed with dichloromethane (2×5 mL). The crude product was obtained by evaporation of the volatiles and purified by centrifugally accelerated thin-layer chromatography with an eluent system of dichloromethane and ethanol ($V_{CH_2Cl_2}/V_{EtOH}$ = 40:1). The fractions containing the product (R_f = 0.24) were combined, and the volatiles evaporated. Yield: 63 mg (73 %).

*General procedure for the synthesis of mononuclear ruthenium(II) complexes **2**–**4***

The appropriate ligand/ligand precursor was suspended in isopropanol (20 mL) and stirred at rt. Dichlorido(η^6-*p*-cymene)ruthenium(II) dimer was added, and the orange reaction mixture was heated to 40 °C (for details see Table I). The suspension turned light orange or yellow and was cooled to –47 °C. The product was precipitated and filtered off (Fig. 2), washed with diethyl ether (4×2 mL) and dried in air.

Properties, analytical and spectral data of the synthesized compounds are given in Supplementary material.

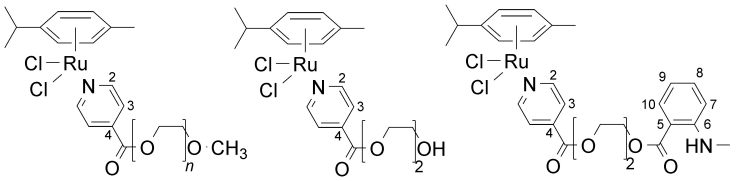

Fig. 2. Chemical structures of mononuclear Ru(II) complexes with ligands **L2**–**L5** (*n* 2–3).

RESULTS AND DISCUSSION

*Poly(ethylene oxide) esters of isonicotinic acid (**L2**–**L4**·HCl and **L5**) and corresponding Ru(II) complexes (**2**–**5**)*

Synthesis. All prepared ligand precursors were synthesised by a similar procedure described in the literature.[28,29] The appropriate acyl chloride was first synthesised by reacting isonicotinic acid with thionyl chloride (Scheme 1). This reaction was catalysed by dimethylformamide (DMF) within 1 h.[30] The proposed

mechanism includes several steps. In the first step, the sulphur atom of thionyl chloride is attacked by the carboxylic acid to give an unstable intermediate, a mixed anhydride. The released hydrogen chloride protonates the carboxylic oxygen atom and makes the carboxylic carbon atom strongly electrophilic. Afterward, the chloride anion attacks the carbon atom, and the intermediate reacts, yielding the desired acyl chloride, sulphur dioxide, and hydrogen chloride.[31,32]

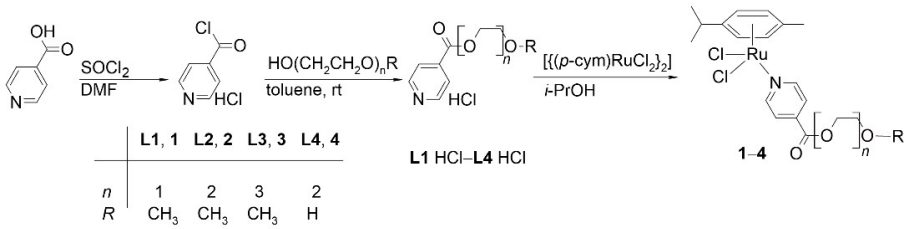

Scheme 1. Synthesis route of poly(ethylene oxide) esters of *iso*nicotinic acid (**L1**–**L4**·HCl).

The acyl chloride was obtained as a light yellow, crystalline powder that reacted exothermically with dried alcohols leading to the release of hydrogen chloride.[33] The reaction mixture, one equivalent acyl chloride with one equivalent alcohol, was stirred at room temperature overnight using dry toluene as solvent (no side products were formed, Scheme 1), yielding the desired product quantitatively.

The structures of ligands were confirmed by the NMR, IR, and ESI-HRMS techniques. The first two are discussed in detail below. The following values were obtained for the mass peaks of the protonated ligands $[L+H]^+$ with the deviation from the calculated values shown in parenthesis: *m*/*z* 226.10738 (**L2**, 0.0 ppm), 270.13351 (**L3**, 0.3 ppm) , 212.09176 (**L4**, 0.3 ppm) and 345.14451 (**L5,** 0.1 ppm).

*Structure and stability of **L1**–**L3** and **1**–**3***. The structures of all ligands optimised at the B3LYP/6-311++G(d,p) level of theory are shown in Fig. 3. This theory level was previously applied to optimize the similar compounds and the spectra assignation.[34,35] As it can be seen, the structure of ligands **L1**–**L3** consists of an aromatic ring adjacent to the ester group and a flexible aliphatic chain (Fig. 3). The planarity of the first part of the compounds is due to the elongated delocalization between the aromatic ring and ester group. In this case, a strong electron donation from the ester group to the aromatic ring is shown in the NBO analysis below. To evaluate the validity of the chosen level of theory for the structural determination of the obtained esters, the optimised bond lengths and angles of previously published **L1**[16] were compared to those of pure isonicotinic acid.[36] This comparison was performed by calculating the mean absolute error (*MAE*) between experimental and theoretical bond lengths and angles. This para-

meter estimates the average absolute difference between two sets of data. The *MAE* values obtained after the comparison are 0.02 Å and 3.1° for bond lengths and angles. The complete list of values is shown in the Supplementary material. After a closer inspection of the data, it is clear that the differences are because isonicotinic acid is in the zwitterionic form in the crystal structure, with the amino group protonated and carboxyl group deprotonated, which leads to the elongation of N−C bonds and equilibration of two C=O bonds. Nevertheless, these results show that the optimized structure resembles the expected crystallographic structure. In case of other two ligands, any significant changes in this part of molecule are not expected. All of the C−O in the aliphatic chain have uniform length of 1.43 Å.

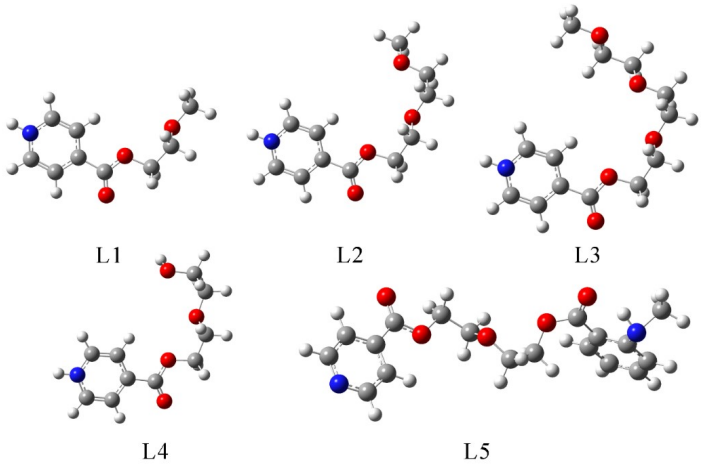

Fig. 3. Optimized ligand structures at B3LYP/6-311++G(d,p) level of theory.

The stability of ligands is governed by intramolecular interactions, as examined in the NBO framework. The most numerous interactions include π(C−C)→ →π*(C−C). These interactions have energies between 95 and 76 kJ mol^{-1} (Table S-I of the Supplementary material). The nitrogen atom is part of the aromatic ring, and its lone pairs are included in the stabilisation of the ring structure. Interactions of the type π(C−N)→π*(C−C) and π(C−C)→π*(C−N) have energies of 60 and 109 kJ mol^{-1}, respectively. The lone pair of nitrogen atoms also stabilise neighbouring C−C atoms, LP(N)→π*(C−C), with the energy of 41 kJ mol^{-1}. The carboxyl group interacts strongly with the aromatic ring. The interconnection between the aromatic ring and carboxylic group is stabilised by the interaction with an energy of 10 kJ mol^{-1}. The planarity of this part of the molecule is possible through strong LP(O)→π*(C−C) interaction with an energy of 75 kJ mol^{-1}. The strongest interactions are within the carboxyl group, LP(O)→

$\rightarrow\pi^*$(C−O), with an energy of 135 kJ mol^{-1}. The rest of the aliphatic chain is stabilised by much weaker interactions that allow free rotation of the groups. The interactions in other ligands are not influenced by the elongation, as these groups are interconnected by the oxygen atoms that act as electron donors to both sides of a chain, but the leakage of electron density is not possible from one side to the other.

The bond is formed between Ru(II) and pyridine nitrogen atom upon complexation. The predicted structures of complexes were optimized at B3LYP/6--31G(d,p)(H, C, O, N, Cl)/LanL2DZ (Ru) level of theory.[37–39] In a previous contribution, this level of theory was applied to [{RuCl(η^6-*p*-cymene)}$_2$(μ-Cl)(μ-1--*N,N'*-naphthyl)]Cl compound and it was shown that the optimised structure represented the crystallographic one well, with the detailed spectra assignment.[10] The optimised structure of **1**, as a representative of the whole class **1**–**3** complexes, is presented in Fig. 4. The optimised structure contains *p*-cymene and **L1** ligand and two chlorine atoms bonded to Ru(II). The resemblance between **L1** and isonicotinoic acid was shown previously, and the same line of reasoning can be applied to the expected similarity between the experimental and the theoretical structures of *p*-cymene moiety.[10] The optimised Ru−Cl bonds have 2.43 and 2.45 Å, almost identical to previously determined lengths in crystal structures of similar compounds.[40] The Ru−N bond length is 2.18 Å, similar to the previously discussed compounds. These bond lengths are not affected by the length of an aliphatic chain of ligands. The optimised bond angles Cl−Ru−Cl and N−Ru−Cl are 90 and 64°, respectively. These angles, again, follow the experimentally determined values. The interactions between Ru(II) and surrounding groups were analysed in the next paragraph through the NBO approach, with the compound **1** given as an example.

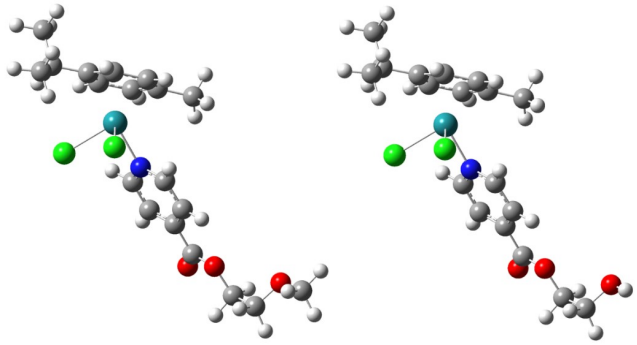

1 4

Fig. 4. Optimized structures of **1** and **4** at B3LYP/6-31+G(d,p)(H,C,N,O,Cl)/LanL2DZ(Ru) level of theory (the following colours represent atoms: white – hydrogen, grey – carbon, blue – nitrogen, green – chlorine, teal – ruthenium).

The stabilisation interactions within the **L1** moiety within **1** are almost identical to those previously discussed. The *p*-cymene moiety contains an aromatic ring with methyl and isopropyl groups. The strongest stabilisation interactions within *p*-cymene denoted as π(C−C)→π*(C−C), have energies between 46 and 55 kJ mol^{-1} (Table S-I). The π electron cloud also interacts with Ru(II) through π(C−C)→LP*(Ru), which includes different carbon-carbon pairs of the aromatic ring. These interactions have energies between 60 and 80 kJ mol^{-1}, proving the Ru(II)-*p*-cymene group's stability. The interactions denoted as LP(Ru)→π*(C−C) were also observed with similar energies. The nitrogen atom of the pyridine ring interacts with Ru(II) through the interactions with an energy of 146 kJ mol^{-1}. The weak interactions denoted as LP(N)→σ*(Ru−Cl) have energies of around 27 kJ mol^{-1}. The carbon–nitrogen bonds stabilize the Ru(II) through π(C−N)→ →LP*(Ru) interactions with energies of 50 kJ mol^{-1}. The stabilisation interaction between nitrogen atom and Ru(II) was observed in other compounds in literature.[41,42] Chlorido ligands also interact with the central metal ion by donating electron pairs. These interactions between lone pairs, LP(Cl)→LP*(Ru), have energies between 34 and 75 kJ mol^{-1}. The weak interactions LP(Cl)→σ(Ru−Cl) of several kJ mol^{-1} stabilise the overall structure. Based on the given values, it can be concluded that the donor atoms, namely chlorine, nitrogen, and aromatic moiety, interact with Ru ions through interactions of similar strength. The aliphatic chain length does not influence these interactions as these groups are further from the interacting nitrogen atom.

Experimental and theoretical NMR spectra. The synthesised **L2**–**L3**·HCl ligands were characterised by NMR spectroscopy. Ligand precursor, previously reported, **L1**·HCl and appropriate ruthenium(II) complex **1**[16] were used for comparison, and the results are given in the mentioned reference. The NMR spectra were modelled for the structures optimized in D_2O and $CDCl_3$ to mimic the experimental conditions. The theoretical chemical shifts were calculated relative to TMS. The experimental and theoretical values for the chemical shifts of **L1**·HCl and **1**, as representative examples, are given in Tables S-II and S-III of the Supplementary material. These values were compared by calculating the *MAE* and correlation coefficient for ^{1}H- and ^{13}C-NMR spectra. The atomic enumeration is shown in Figs. 1 and 2, and it should be remembered that the aromatic carbon atoms are symmetric; therefore, a lower number of resonances is observed.

The results from Tables S-II and S-III show that the theoretical chemical shifts are in agreement with the experimental ones. The calculated values were overestimated, and the correction factor was obtained from the dependency between experimental and theoretical values (0.94 for ^{1}H- and 0.97 for ^{13}C--NMR). When ^{1}H-NMR spectra are concerned, the correlation factors between the two sets of values were 0.97/0.99 for **L1·HCl** and **1**. The *MAE* value was

0.27 ppm in the case of **L1**·HCl and 0.44 ppm in the case of **1**. These high correlation factors and low *MAE* values result from the relative rigidity of the overall structure represented by aromatic rings and structures with elongated delocalisation. These results prove the applicability of the selected level of theory for the representation of the newly obtained Ru(II) complexes. The lowest value of chemical shifts was obtained for the methoxy group in the aliphatic chain (3.48 ppm in the experimental and 3.28 ppm in the theoretical spectrum). The proximity of oxygen atoms increased chemical shifts to 3.92 ($OC\underline{H}_2$) and 4.67 ($COOC\underline{H}_2$) ppm in the experimental spectrum. These values are, on average, 0.3 ppm different in the theoretical spectrum. In the pyridine ring, the appropriate chemical shifts are much higher and depend on the proximity of the nitrogen atom. Two sets of resonances at 8.62 and 9.05 ppm represent the hydrogen atoms in the experimental spectrum. Once the complex is formed, the largest difference was observed for the hydrogen atoms adjacent to nitrogen (9.23 *vs*. 9.05 ppm, and 7.86 *vs*. 8.62 ppm), proving that a new interaction between nitrogen and Ru(II) is formed, inducing the changes in the electron density of the ring. The ^{1}H-NMR chemical shifts of protons form the *p*-cymene moiety have the expected values common for other similar compounds.[40]

The ^{13}C-NMR chemical shifts are more commonly used for the comparison due to the lower possibility for rotation. In the ligand structure, the lowest chemical shifts were obtained for the carbon atoms of the aliphatic chain (58.2 ($O\underline{C}H_3$), 65.9 ($\underline{C}H_2OOC$) and 69.6 ($\underline{C}H_2O$) ppm). These carbon atoms are located at 62.8, 73.9, and 73.7 ppm in the theoretical spectrum. The presence of two oxygen atoms in the carboxyl group significantly increases the chemical shift value to 163.4 in the experimental and 161.4 ppm in the theoretical spectrum. Carbon atoms of the pyridine ring also have the expected values. The carbon atoms adjacent to nitrogen in the pyridine ring increase the chemical shift value upon complexation (142.7 to 155.9 ppm). The rest of the carbon atoms retain the position of the resonances present in **L1**·HCl. The same applies to chemical shifts of carbon atoms in the *p*-cymene moiety.

Experimental and theoretical IR spectra. The experimental and theoretical IR spectra were also compared in order to investigate the applicability of the selected level of theory. The theoretical vibrational motion was visualised in GausView,[22] as previously mentioned. The theoretical wavenumber values were overestimated, and the correction factors suggested by the National Institute for Standards and Technology (NIST) for the given level of theory were used. The IR spectra of **L1**·HCl and **1** will be discussed as the representative examples of ligands **L1**–**L3**·HCl and complexes **1**–**3**. The detailed spectral characterisation for other ligands and complexes is presented under the synthetic procedure and characterisation in the previous Methodology section.

The IR spectrum of **L1**·HCl contains four characteristic bands found at approximately 1730, 1280, 1110 and 750 cm^{-1}. The first band at 1730 cm^{-1} in the experimental spectrum is assigned to the C=O ester group vibration. In the theoretical spectrum, this band is positioned at 1756 cm^{-1}, which is well reproduced, bearing in mind that the IR spectrum was recorded for a solid sample, and the theoretical calculations were performed for an isolated compound. The band at 1280 cm^{-1} is a typical absorption band for carbon–oxygen single bonds in ether and ester groups[43] This C–O stretching vibration in the theoretical spectrum is at 1270 cm^{-1}. The strong, broad band at 1110/1123 cm^{-1} in the experimental/theoretical spectra of **L1**·HCl corresponds to the ester/ether vibration. The band at approximately 750 cm^{-1} results from vibrations of the pyridine ring in both spectra but can be overlapped by carbon-hydrogen vibrations in the fingerprint region.[44]

Further specific bands, which are weaker in the spectra, are observed near 3020 cm^{-1} for heteroaromatic vibrations and near 2980 cm^{-1} for alkyl groups of the poly(ethylene oxide) spacer.[44] The positions of these bands are also similar in the theoretical spectrum. In the IR spectrum of **1**, the most prominent bands are located at 1730, 1275 and 1119 cm^{-1}, almost identical to the previously discussed values. A new strong band is positioned at 276 cm^{-1}, corresponding to the Ru–Cl stretching vibration. The similar values were obtained for the trichloridotriaquoruthenium(III) complex[45].

*2-(2-Hydroxyethoxy)ethyl ester of isonicotinic acid (**L4**·HCl) and corresponding Ru(II) complex (**4**)*

Synthesis. The appropriate acyl chloride hydrochloride was obtained using the modified method for **L1**·2HCl–**L3**·HCl. The synthesis is changed using excess alcohol to the acyl chloride hydrochloride (6 eq.) in toluene. The crude product is obtained as viscous oil with a high percentage of diethylene glycol and small amounts of **L1**·2HCl or **L4**·2HCl. The product is extracted with acetone/ /diethyl ether ($V_{Acetone}/V_{Et2O}$ = 5:1) and precipitated with diethyl ether several times. ESI–HRMS analysis was performed under the same conditions as **L1**·HCl. Results showed the expected mass peaks of the $[M+H]^+$.

*Structure and stability of **L4**·HCl and **4***. The structures of **L4**·HCl and **4** are presented in Figs. 3 and 4. The structure of **L4**·HCl greatly resembles the structure of **L2**·HCl, but the methoxy group is exchanged with the hydroxyl group. This change is not expected to influence the stability and structural features of the ligand significantly. The weaker stabilisation interaction was obtained in the aliphatic chain (LP(O)→σ(C–C)), with an energy of 4.8 in **L4**·HCl *vs.* 5.1 kJ mol^{-1} in **L1**·HCl (Table S-I). This change in the group does not influence the complexation route and the geometry of the complex **4** compared to **2**.

Experimental and theoretical NMR spectra. The experimental and theoretical NMR spectra of **L4**·HCl and **4** also resemble those previously mentioned in

L2·HCl and **2**. The NMR chemical shifts of **L4**·HCl and **4** are presented in Tables S-IV and S-V of the Supplementary material. As in the previous case, the obtained values were overestimated, and the correction coefficients were determined as the slope in the dependency of experimental on theoretical values. In the ^{1}H-NMR spectrum of **L4**·HCl, four hydrogen atoms of the aliphatic chain (HOC$\underline{H_2}$C$\underline{H_2}$) have the same chemical shifts at 3.77 ppm in the experimental spectrum. In the theoretical spectrum, the chemical environments of these protons are different due to the calculations performed for the compounds in vacuum and without free rotation. Other hydrogen atoms have their expected positions. The hydrogen atom of the OH group was not observed in the experimental range. The carbon atom adjacent to OH has a higher chemical shift value than the corresponding one with OCH_3 group (in **L2**·HCl; 71.8 *vs*. 69.6 ppm). The MAE values for ^{1}H- and ^{13}C-NMR spectra of **L4**·HCl are 0.24 and 4.1 ppm, with high correlation coefficients ($R > 0.98$). Upon the formation of **4**, the most notable differences are observed in the chemical shifts of carbon atoms in the pyridine ring. The *MAE* value for ^{13}C-NMR chemical shifts is 4.5 ppm, with *R* equal to 0.98. A higher *R*-value was calculated for ^{1}H-NMR chemical shifts of **4**. These results prove the applicability of the chosen level of theory for the representation of both ligand and complex.

Experimental and theoretical IR spectra. The experimental and theoretical IR spectra were compared as additional proof of the structural representation of **L4**·HCl and **4**. The same method was applied for the correction of theoretical wavenumber values. The IR spectrum **L4**·HCl is characterised by a broad peak at 3350 cm^{-1} attributed to the O−H stretching vibration. In the theoretical spectrum, this band is shown at 3737 cm^{-1}. This difference is expected as the optimization was performed on the isolated molecule in a vacuum. When the intermolecular interactions are formed, the O−H bond length increases, and the wavenumber lowers. The most intense peak is at 1730 in the experimental and 1755 cm^{-1} in the theoretical spectra of **L4**·HCl, assigned to the C=O vibration. The vibrations of carbon–oxygen bonds at 1280 and 1110 cm^{-1} are similar to those previously discussed for **L1**·HCl. The heteroaromatic vibrations at 750 cm^{-1} are observed in the same region as the bands of other ligand precursors (**L1**·2HCl–**L3**·HCl). These results correlate well with all other synthesised esters. In the experimental and theoretical spectra of **4**, the bands of aliphatic and aromatic C−H stretching vibrations increase in intensity due to *p*-cymene moiety. The remaining bands are not significantly affected except for forming new bands assigned to Ru−Cl vibrations.

*2-[2-(2-Methylamino-benzoyloxy)ethoxy]ethyl isonicotinate (**L5**) and corresponding Ru(II) complex (**5**)*

Synthesis. Ligand **L5** was prepared in the reaction between **L4**·HCl and methylisatoic acid anhydride in the presence of potassium carbonate, as pre-

sented below. The reaction mixture was stirred for three hours at 60 °C in acetonitrile, and the reaction progress was followed with thin-layer chromatography (Scheme 2). Another reaction setup with toluene as solvent and at a higher temperature yielded only small amounts of the desired product. The crude product was purified by the centrifugally accelerated thin-layer chromatography with an eluent system of dichloromethane and ethanol. The analysis with ESI-HRMS resulted in the expected mass peak of the protonated molecule (m/z = 345.14451) $[M+H]^+$. The product was obtained in good yield (73 %).

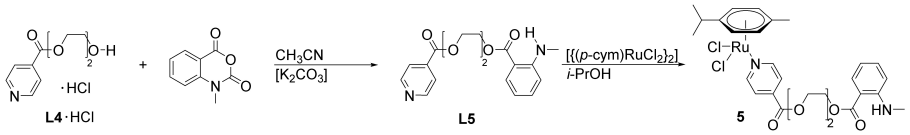

Scheme 2. Preparation of the fluorescent ligand **L5** and corresponding ruthenium(II) complex (**5**).

*Structure and stability of **L5** and **5***. The optimised structures of **L5** and **5** are shown in Figs. 3 and 5. Ligand **L5** has the most complex structure of the described compounds, as there is an additional condensed structure of methylisatoic acid moiety attached to the PEG chain. As previously discussed, the complexation does not influence the stabilisation interactions within the ligand structure; therefore, the NBO analysis of **L5** and **5** is shown together. Besides stabilisation interactions in the pyridine ring, aliphatic chain, and *p*-cymene moiety, strong interactions were observed at the intersection of the aliphatic chain and methylisatonic acid moiety. The lone pair on the carboxylic oxygen atom stabilises the neighbouring C–O and C–C bonds by 132 and 71 kJ mol^{-1}, respectively (Table S-I). The adjacent oxygen atom stabilises the carboxylic group through the

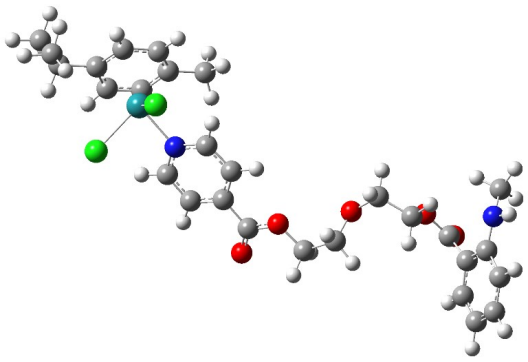

Fig. 5. Optimized structure of **5** at B3LYP/6-31+G(d,p)(H,C,N,O,Cl)/LanL2DZ(Ru) level of theory (the following colours represent atoms: white –hydrogen, grey – carbon, blue – nitrogen, green – chlorine, teal – ruthenium).

LP(O)→π*(C−O) interaction with energy equal to 105 kJ mol^{-1}. The stabilisation interactions within the aromatic ring have similar energies to those of pyridine and *p*-cymene moieties, between 45 and 55 kJ mol^{-1}. The nitrogen atom increases the stability of this ring through the positive resonance effect and the electron delocalisation. Including these groups does not influence the part of the ligand directly attached to Ru(II), as there is a long chain with the electronegative atom intersections that prevents electron delocalisation through the entire molecule. The structure of the ligand and the corresponding complex is further analysed by NMR and IR spectroscopies.

Experimental and theoretical NMR spectra. The NMR spectra of **L5** and **5** are given in the Supplementary material (Tables S-VI and S-VII). The ^{1}H-NMR spectrum of **5** shows several changes and additional resonances compared to the characterised ligand precursor (**L4**·HCl). First, the resonances of the isonicotinate moiety are shifted to a higher field ($\Delta\delta(H^2)$ = –0.3 ppm, $\Delta\delta(H^3)$ = –0.8 ppm). The corresponding carbon atoms give resonances, which are observed in almost the same position as the earlier discussed free ligands (**L5**: $\delta(C^2)$ = 149.8 ppm, $\delta(C^3)$ = 123.4 ppm, **L4**·HCl: $\delta(C^2)$ = 149.4 ppm, $\delta(C^3)$ = 123.0 ppm). Additionally to the previously described ligand precursors herein, in ^{13}C-NMR spectra there is the presence of two chemical shifts above 160 ppm (164.9 and 168.5 ppm) corresponding to COO and CON groups from isonicotinic and methylisatoic moieties, respectively. Two resonances near 4.5 ppm are assigned to protons, which directly bond to the ester groups and show no coupling with each other. More resonances are observed for the new aromatic system, the fluorescent group. The chemical shifts belonging to the aromatic regions of the fluorescent moiety range from 6.5–7.9 ppm. One doublet of the fluorescent moiety is shifted to approximately 7.9 ppm (compared to methylisatoic acid anhydride) and overlaps with the doublet of the isonicotinate group at 7.8 ppm. Another resonance for the methyl group bound to the nitrogen atom of the amine pendant group is found at 2.9 ppm. The theoretical spectrum of **L5** at B3LYP/6-311++G(d,p) level of theory reproduces well the experimental one. The *MAE* values for ^{1}H- and ^{13}C-NMR spectra are 0.40 and 4.3 ppm, which aligns with the previous predictions of other ligands. The most notable differences in the calculated spectrum were observed for the carboxyl carbon atoms, averaging 6 ppm. When **5** is formed, the differences in chemical shifts were obtained for the carbon atoms adjacent to the nitrogen atom of the pyridine ring. These shifts were 6 ppm (149.8 in **L5** and 155.9 ppm in **5**). The rest of the carbon and hydrogen atoms do not show significant changes. The correlation coefficients between the experimental and the theoretical chemical shifts are 0.94 and 0.95 for ^{1}H- and ^{13}C--spectra, with *MAE* values of 0.79 and 6.0 ppm. These results again prove the theoretical representation of ligand and complex, even when the elongated structure of **L5** is concerned.

Experimental and theoretical IR spectra. In addition to the specific bands observed at 1718 cm^{-1} for the carbonyl group of the isonicotinate part, at 1260 and 1120 cm^{-1} for carbon–oxygen bonds and 750 cm^{-1} for aromatic bending vibrations, two strong bands are significant for this ligand precursor. The first new sharp band at 3370 cm^{-1} can be assigned to a stretching vibration of the secondary amine.[43] This band is located at 3382 cm^{-1} (scaled) in the theoretical spectrum. The difference of 18 cm^{-1} is due to the physical state of the recorded sample, but it is still within the expected difference. The second strong band at 1684 cm^{-1} is generated by the carbonyl stretching vibration of the newly formed ester bond of the fluorescent benzene ring and is observed in other esters of *N*--methylisatoic anhydride, too.[46,47] The band assigned to this vibration in the theoretical spectrum is 1648 cm^{-1}. The vibration of this carboxyl group is lower than the one previously observed in ligands **L1**–**L4**·HCl due to the proximity of the aromatic ring, which extends the electron delocalisation and elongates the respective C=O band. These bands characteristic of ligand are positioned at 3372 and 1676 cm^{-1} in the experimental spectrum of **5**, which proves the assumption that this part of the ligand is not under the influence of metal ions, as shown previously in the NMR spectrum. In the theoretical spectrum, these wavenumbers are higher for several cm^{-1} but within the expected range.

*Experimental and theoretical UV–Vis/fluorescence spectra of **L5***. The UV––Vis and fluorescence spectra of **L5** and **5** in $CHCl_3$ are presented in Fig. 6. The UV–Vis spectrum of **L5** has a broad peak at 355 nm. The emission spectrum is measured with an excitation wavelength of 372 nm and in a range from 387–550 nm. The excitation pattern was analysed with an emission wavelength of 418 nm from 200–400 nm. Ligand **L5** shows a broad excitation spectrum, and the maximum excitation intensity is at 371 nm, additionally, two shoulders are observed at 342 and 266 nm. The first shoulder at a lower wavelength shows a high intensity and reaches 89 % of the intensity of the peak at 371 nm. The second shoulder is weaker and reaches only 24 % of the highest intensity. Due to these two shoulders, the excitation spectrum ranges approximately 160 nm (240–400 nm). Complex **5** shows peaks at the same position, just their intensity is much lower that of those in **L5** spectrum. Similarity in position can be explained by the weak influence of the metal ion on the overall electron density of the groups included in the transitions. The decrease in intensity is due to the competing deactivation processes and the energy dissipation through vibration and partial rotation.

The structure of **L5** optimized at B3LYP/6-311++G(d,p) level of theory in $CHCl_3$ was used to predict the electronic spectrum. In the range of experimental values, the theoretical spectrum is dominated by an intensive peak at 344 nm, assigned to HOMO→LUMO (99 %) transition, with an oscillator strength of 0.1283. The calculated wavelength differs by around 10 nm from the experimental one, and it can be assumed that the interactions with the solvent would inf-

luence an additional shift in the spectrum, although strong interactions with $CHCl_3$ are not expected due to the low solvent's low dipole moment. In the theoretical spectrum of **5** a much higher number of weak transitions can be observed. These transitions are attributed to the metal-ligand electron transitions. The most intense transition is positioned at 360 nm, with the oscillator strength of 0.1165, denoted as HOMO→LUMO+3 (97 %). This result shows that the experimental value of 355 nm is well-reproduced in the theoretical spectrum of **5**. Also, a shift between theoretical values of transitions assigned to ligand can be a consequence of the level of theory used and change in electron density upon complexation.

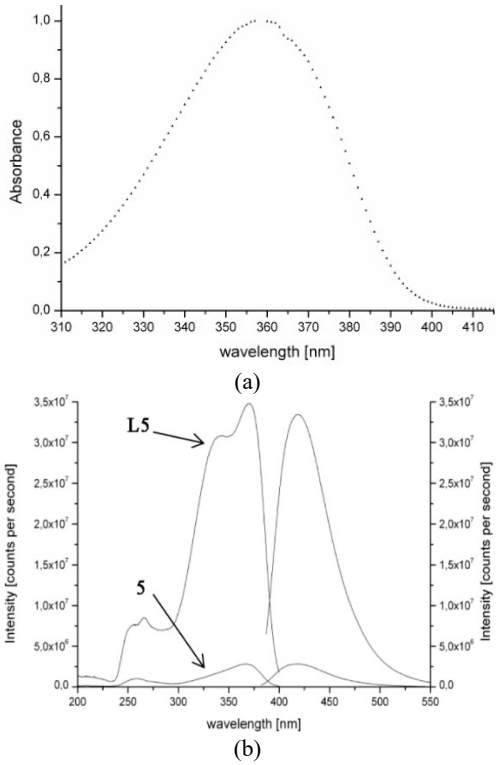

Fig. 6. UV–Vis/fluorescence spectra of ligand **L5** (a) and **5** (b).

CONCLUSION

Ligands **L2**–**L4**·HCl were prepared in the reaction between appropriate acyl chloride and dried alcohols. The theoretical structures, including already reported **L1**·HCl, were obtained at the B3LYP/6-31+G(d,p)(H,C,N,O,Cl)/LanL2DZ(Ru) level of theory. Due to the elongated delocalisation between the aromatic ring and ester group, the strongest stabilisation interactions included π(C−C)→ →π*(C−C) and LP(O)→π*(C−C), as determined by the NBO approach. The pyr-

idine ring was also stabilised by the LP(N)→π*(C−C), with an energy of 41 kJ mol^{-1}. The bond is formed between Ru(II) and pyridine nitrogen upon complexation. Two Ru−Cl bonds have 2.43 and 2.45 Å, while the Ru−N bond length was 2.18 Å. The optimised bond angles were in the expected range. High correlation coefficients (>0.98) were calculated for the experimental and theoretical ^{1}H- and ^{13}C-NMR chemical shifts. As a representative example, the *MAE* values were 0.23 and 4.3 ppm for ^{1}H- and ^{13}C-NMR spectra of **L1**. The IR spectra were well reproduced, with differences explained by the physical state of the substance. The NMR and IR spectra of **L4**·HCl and the corresponding complex **4** also proved the applicability of the chosen theory of level. The additional moiety in ligand **L5** led to high-intensity fluorescent emission. This group was stabilised by the interactions between carboxyl group and π-electron cloud of aromatic ring. The fluorescence emission peak of **L5** was obtained at 372 nm for the excitation wavelength of 418 nm. The experimental and theoretical wavelengths of the most intense transition in the UV–Vis spectrum of **L5** were 355 and 344 nm, respectively. Much more successful overlap between the experimental and the theoretical values was obtained for the UV–Vis spectrum of **5**, with 5 nm difference. This difference was explained by the stabilisation due to the solvent-solute interactions. As the stability and the structure of these compounds were obtained, further biological activity studies are advised.

SUPPLEMENTARY MATERIAL

Additional data and information are available electronically at the pages of journal website: https://www.shd-pub.org.rs/index.php/JSCS/article/view/12353, or from the corresponding author on request.

ИЗВОД

СИНТЕЗА, СПЕКТРОСКОПСКА И DFT АНАЛИЗА ДИХЛОРИДО(η^6-*p*-ЦИМЕН)РУТЕНИЈУМ(II) КОМПЛЕКСА СА ИЗОНИКОТИНАТ-ПОЛИЕТИЛЕН ГЛИКОЛ ЕСТАРСКИМ ЛИГАНДИМА

THOMAS EICHHORN[1], ДУШАН ДИМИЋ[2], ЗОРАН МАРКОВИЋ[3] и ГОРАН Н. КАЛУЂЕРОВИЋ[1]

[1]Department of Engineering and Natural Sciences, University of Applied Sciences Merseburg, Eberhard-Leibnitz-Straße 2, 06217 Merseburg, Germany, [2]Универзитет у Београду, Факултет за физичку хемију, Студентски трг 12–16, 11000 Београд [3]Институт за информационе технологије, Универзитет у Крагујевцу, Јована Цвијића бб, 34000 Крагујевац

Комплекси рутенијума су значајни због рутенијумове сличности гвожђу, мање токсичности, и веће антиканцер ефикасности. У овом раду, пет нових изоникотинат-полиетилен-гликол естарских лиганада је синтетисано и окарактерисано NMR и IC спекроскопијама. Одговарајући Ru(II) комплекси су такође добијени и њихова структура одређена стандардним методама. Оптимизација структуре је урађена на B3LYP/6-31+G(d,p) нивоу теорије за H, C, N и O атоме и B3LYP/LanL2DZ за Ru. Интрамолекулске стабилизационе интеракције су испитане анализом природних орбитала. Хемијски помераји у NMR спектрима су предвиђени GIAO (*gauge independent atomic orbital*) методом и упоређени са експерименталним вредностима. Високи коефицијент корелације и ниска средња вредност апсолутне разлике између ових скупова вредности доказују да пред-

виђене структуре добро описују експерименталне. Теоријски и експериментални IC спектри су такође упоређени, а разлике у положајима трака објашњене. Један од лиганада (**L5**) и комплекса (**5**) је показао флуоресцентне особине због присуства метилисатоичне групе. Електронски спектри овог једињења су моделовани временски зависном DFT методом. Разлика од 11 nm између експерименталне и теоријске таласне дужине је објашњена интеракцијама између растворка и растварача. За ову серију једињења су препоручене даље биолошке и теоријске анализе.

(Примљено 12. априла, ревидирано 26. јуна, прихваћено 18. септембра 2023)

REFERENCES

1. R. G. Kenny, C. J. Marmion, *Chem. Rev.* **119** (2019) 1058 (https://doi.org/10.1021/acs.chemrev.8b00271)
2. T. C. Johnstone, K. Suntharalingam, S. J. Lippard, *Chem. Rev.* **116** (2016) 3436 (https://doi.org/10.1021/acs.chemrev.5b00597)
3. S. Thota, D. A. Rodrigues, D. C. Crans, E. J. Barreiro, *J. Med. Chem.* **61** (2018) 5805 (https://doi.org/10.1021/acs.jmedchem.7b01689)
4. A. Rilak Simović, R. Masnikosa, I. Bratsos, E. Alessio, *Coord. Chem. Rev.* **398** (2019) 113011 (https://doi.org/10.1016/j.ccr.2019.07.008)
5. L. Conti, E. Macedi, C. Giorgi, B. Valtancoli, V. Fusi, *Coord. Chem. Rev.* **469** (2022) 214656 (https://doi.org/10.1016/j.ccr.2022.214656)
6. S. Y. Lee, C. Y. Kim, T.-G. Nam, *Drug Des. Devel. Ther.* **14** (2020) 5375 (https://doi.org/10.2147/DDDT.S275007)
7. B. Therrien, *Coord. Chem. Rev.* **253** (2009) 493 (https://doi.org/10.1016/j.ccr.2008.04.014)
8. M. J. Clarke, *Coord. Chem. Rev.* **232** (2002) 69 (https://doi.org/10.1016/S0010-8545(02)00025-5)
9. G. S. Smith, B. Therrien, *Dalt. Trans.* **40** (2011) 10793 (https://doi.org/10.1039/C1DT11007A)
10. D. S. Dimić, G. N. Kaluđerović, E. H. Avdović, D. A. Milenković, M. N. Živanović, I. Potočňák, E. Samoľová, M. S. Dimitrijević, L. Saso, Z. S. Marković, J. M. Dimitrić Marković, *Int. J. Mol. Sci.* **23** (2022) 1001 (https://doi.org/10.3390/ijms23021001)
11. G. Jia, G.-L. Law, K.-L. Wong, P. A. Tanner, W.-T. Wong, *Inorg. Chem.* **47** (2008) 9431 (https://doi.org/10.1021/ic8010103)
12. R. Schobert, B. Biersack, *Inorg. Chim. Acta* **358** (2005) 3369 (https://doi.org/10.1016/j.ica.2005.05.015)
13. L. D. Ramos, G. Cerchiaro, K. P. Morelli Frin, *Inorg. Chim. Acta* **501** (2020) 119329 (https://doi.org/10.1016/j.ica.2019.119329)
14. C.-M. Wang, Y.-L. Chuang, S.-T. Chuang, K.-H. Lii, *J. Solid State Chem.* **177** (2004) 2305 (https://doi.org/10.1016/j.jssc.2004.02.030)
15. J.-Y. Kim, A. J. Norquist, D. O'Hare, *Chem. Mater.* **15** (2003) 1970 (https://doi.org/10.1021/cm021722n)
16. T. Eichhorn, E. Hey-Hawkins, D. Maksimović-Ivanić, M. Mojić, J. Schmidt, S. Mijatović, H. Schmidt, G. N. Kaluderović, *Appl. Organomet. Chem.* **29** (2015) 20 (https://doi.org/10.1002/aoc.3238)
17. *Gaussian 09, Revision A.02*, Gaussian Inc., Wallingford, CT, 2009
18. A. D. Becke, *J. Chem. Phys.* **98** (1993) 5648 (https://doi.org/10.1063/1.464913)
19. T. H. Dunning, *J. Chem. Phys.* **90** (1989) 1007 (https://doi.org/10.1063/1.456153)
20. P. J. Hay, W. R. Wadt, *J. Chem. Phys.* **82** (1985) 299 (https://doi.org/10.1063/1.448975)

21. P. J. Hay, W. R. Wadt, *J. Chem. Phys.* **82** (1985) 270 (https://doi.org/10.1063/1.448799)
22. R. Dennington, K. Todd, J. Millam, *Gauss View, Version 5*, Semichem Inc., Shawnee, KS, 2009
23. A. V. Marenich, C. J. Cramer, D. G. Truhlar, *J. Phys. Chem., B* **113** (2009) 6378 (https://doi.org/10.1021/jp810292n)
24. A. E. Reed, R. B. Weinstock, F. Weinhold, *J. Chem. Phys.* **83** (1985) 735 (https://doi.org/10.1063/1.449486)
25. R. Zieliński, H. Szymusiak, *Pol. J. Food Nutr. Sci.* **12** (2003) 157 (http://journal.pan.olsztyn.pl/pdf-98612-30420?filename=APPLICATION%20OF%20DFT.pdf)
26. J. A. Bohmann, F. Weinhold, T. C. Farrar, *J. Chem. Phys.* **107** (1997) 1173 (https://doi.org/10.1063/1.474464)
27. D. Jacquemin, J. Preat, V. Wathelet, E. A. Perpète, *Chem. Phys.* **328** (2006) 324 (https://doi.org/10.1016/j.chemphys.2006.07.037)
28. G. R. Newkome, K. J. Theriot, V. K. Gupta, R. N. Balz, F. R. Fronczek, *Inorg. Chim. Acta* **114** (1986) 21 (https://doi.org/10.1016/S0020-1693(00)84582-X)
29. C. O. Badgett, C. F. Woodward, *J. Am. Chem. Soc.* **69** (1947) 2907 (https://doi.org/10.1021/ja01203a501)
30. H. H. Bosshard, R. Mory, M. Schmid, H. Zollinger, *Helv. Chim. Acta* **42** (1959) 1653 (https://doi.org/10.1002/hlca.19590420526)
31. J. Clayden, N. Greeves, S. Warren, *Organic Chemistry*, 2nd ed., Oxford University Press, Oxford, 2012 (ISBN: 978-0-19-927029-3)
32. A. Wollrab, *Organische Chemie*, 2nd ed., Springer Verlag, Berlin, 2012 (ISBN:978-3-642-45143-0)
33. *Organikum*, 22nd ed., Wiley VCH, Weinheim, 2004 (ISBN: 978-3-527-33968-6)
34. G. Świderski, M. Kalinowska, R. Świsłocka, S. Wojtulewski, W. Lewandowski, *Spectrochim. Acta, A* **100** (2013) 41 (https://doi.org/10.1016/j.saa.2012.02.047)
35. S. Ramalingam, S. Periandy, S. Mohan, *Spectrochim. Acta, A* **77** (2010) 73 (https://doi.org/10.1016/j.saa.2010.04.027))
36. A. G. Medvedev, A. A. Mikhailov, P. V. Prikhodchenko, T. A. Tripol'skaya, O. Lev, A. V. Churakov, *Russ. Chem. Bull.* **62** (2013) 1871 (https://link.springer.com/article/10.1007/s11172-013-0269-9)
37. M. Al-Noaimi, M. A. AlDamen, *Inorg. Chim. Acta* **387** (2012) 45 (https://doi.org/10.1016/j.ica.2011.12.050)
38. V. Uahengo, P. Cai, J. Naimhwaka, A. Rahman, L. S. Daniel, H. Bhakhoa, L. Rhyman, P. Ramasami, *Polyhedron* **173** (2019) 114106 (https://doi.org/10.1016/j.poly.2019.114106)
39. A. A. Sikalov, V. V. Pavlovskiy, A. A. Kirilchuk, *Inorg. Chem. Commun.* **99** (2019) 156 (https://doi.org/10.1016/j.inoche.2018.11.020)
40. T. Eichhorn, F. Kolbe, S. Mišić, D. Dimić, I. Morgan, M. Saoud, D. Milenković, Z. Marković, T. Rüffer, J. Dimitrić Marković, G. N. Kaluđerović, *Int. J. Mol. Sci.* **24** (2023) 689 (https://doi.org/10.3390/ijms24010689)
41. A. Mondal, U. Sen, N. Roy, V. Muthukumar, S. K. Sahoo, B. Bose, P. Paira, *Dalt. Trans.* **50** (2021) 979 (https://doi.org/10.1039/D0DT03107K)
42. M. T. Rupp, N. Shevchenko, G. S. Hanan, D. G. Kurth, *Coord. Chem. Rev.* **446** (2021) 214127 (https://doi.org/10.1016/j.ccr.2021.214127)
43. E. Pretsch, P. Bühlmann, C. Affolter, *Structure Determination of organic compounds*, 3rd ed., Springer Verlag, Berlin, 2000 (ISBN: 978-3-662-62439-5)

44. M. Hesse, H. Meier, B. Zeeh, *Spektroskopische Methoden in der organischen Chemie*, 7th ed., Georg Thieme Verlag, Stuttgart, 2002 (http://dx.doi.org/10.1055/b-002-46985)
45. J. R. Durig, W. A. McAllister, E. E. Mercer, *J. Inorg. Nucl. Chem.* **29** (1967) 1441 (https://doi.org/10.1016/0022-1902(67)80244-6)
46. I. Chevrier, J. L. Sagué, P. S. Brunetto, N. Khanna, Z. Rajacic, K. M. Fromm, *Dalton Trans.* **42** (2013) 217 (https://doi.org/10.1039/C2DT31259J)
47. D. Roell, T. W. Rösler, S. Degen, R. Matusch, A. Baniahmad, *Chem. Biol. Drug Des.* **77** (2011) 450. (https://doi.org/10.1111/j.1747-0285.2011.01116.x).